Improved Frequency Stability Support for Low-Inertia Power Systems

Improved Frequency Stability Support for Low-Inertia Power Systems

Hannu Laaksonen
School of Technology and Innovations
University of Vaasa
Vaasa, Finland
hannu.laaksonen@uwasa.fi

***Abstract*—In the renewable generation -based low-inertia power systems, frequency stability support from different types and sizes of inverter-based distributed energy resources (DERs) is of major importance. Various grid-following and -forming inverter synchronization and control methods will affect the frequency stability in different ways. In this paper, frequency stability supporting improved active power response of inverter-connected DER having synchronization based on universal frequency locked loop (U-FLL) is presented. U-FLL-based synchronization as well as active power–frequency (*Pf*) -droop control is further modified to achieve faster response and better frequency stability support from the studied battery energy storage system (BESS). In addition, this paper shows frequency stability comparison of U-FLL-based BESS and four grid-forming (GFM) control methods on PV-based DER unit. In the case studies with PSCAD simulation software, simplified hybrid power system model with synchronous generation and inverter-based resources (IBRs) are used to study the effect of IBRs i.e. BESS or PV on frequency stability after a load increase.**

***Index Terms*—Frequency stability, Low-Inertia Power System, Grid-forming, Inverter-based Resources, Active Power Control**

I. INTRODUCTION

Traditional synchronization and control of IBRs use grid-following (GFL) methods for the control based on the assumption that voltage and frequency of the power system are mainly determined by the high-inertia synchronous generators (SGs). In the future, however, the GFM IBRs' share must be large enough to enable frequency stability management and upkeep in the power systems after sudden disturbances or changes in the generation, consumption or network topology also during low-inertia situations. Typically, GFL IBR is defined as a current source and GFM IBR as a voltage source. However, there does not exist any definition for GFM control which is generally accepted, and various methods have been proposed previously. [1]-[6]

One key difference between GFL and GFM IBRs is the synchronization which affects also to their stability and behaviour during and after disturbances. Synchronization of GFL IBR to the power system's frequency and voltage angle is commonly done by frequency-locked-loop (FLL) or phase-locked-loop (PLL) component. Many GFM IBRs do not have FLL or PLL and synchronization of them is done, for instance, by droop control. Slow response of active power (*P*) -based frequency support services from *Pf*-droop -controlled GFL IBRs due to filtering of the frequency measurement have been one concern in power systems with low-inertia. Therefore, few quite recent network codes have also required voltage source or SG type of rapid *P* support from larger GFM IBRs during disturbance events for improved power system's stability support.

In the past studies [7]-[14], U-FLL -based grid-supporting and -forming synchronization method has been presented for different type of DERs. U-FLL could also directly replace the existing PLL-component of GFL IBRs including also demand-type of DERs. In this paper, U-FLL-based synchronization and *Pf*-droop control of IBRs is further improved from the previous studies [7]-[14] to achieve faster response and better frequency stability support from the studied BESS. This paper shows also frequency stability comparison of U-FLL-based BESS and four different GFM control methods (Synchronous reference frame (SRF)-PLL, Virtual Synchronous Machine (VSM), Droop and Dispatchable Virtual Oscillator Control (dVOC)) with PV-based DER using detailed scaled IBR model from [15]. In the PSCAD simulations, simple power system model with SG and BESS or GFM PV is used to study their effect on the power system frequency stability after a load increase.

II. STUDY SYSTEM AND CASES

The studied power system is presented in Fig. 1. This small HV network includes one large SG as well as BESS or PV depending on the study case (see Tables I and II) connected close to the SG (Fig. 1). PSCAD model of the HV grid-connected SG is presented with more details in [10]. 20 MW BESS's (Fig. 1) simplified PSCAD model based on controlled voltage sources as well as the utilized controlling scheme including the synchronization with U-FLL component is shown with more details in [10]. Fig. 2 shows the further modified U-FLL component from [11] that is used in the simulations of this paper with the 20 MW BESS (Fig. 1, Table

I). Then, in Fig. 3a) the simulated 20 MW BESS's *Pf*-droop is presented for one 4 MW BESS because the 20 MW (5*4 MW) BESS consists of five similar parallel 4 MW BESS units. Fig. 3b) shows the input frequency filtering including moving averaging (75 + 75 ms) and rate limiter of the BESS's *Pf*-droop control when the input frequency is coming from the FFT -block of PSCAD like in [10]. In Fig. 3c), BESS's further modified *Pf*-droop from Fig. 3b) and [10] is presented. Fig 3d) shows the input frequency filtering (5 ms moving average) of the BESS *Pf*-droop control when the input comes from SG speed as also presented in [10]. The main aim of the studied and proposed new modifications to the U-FLL-based synchronization (Fig. 2) and *Pf*-droop control (Fig. 3c) from the previous studies [7]-[14] is to achieve improved support for frequency stability by faster *P* response from the studied BESS unit.

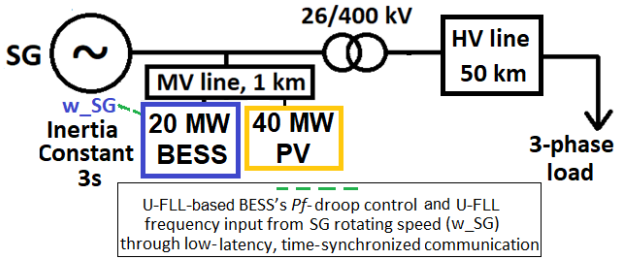

Figure 1. Studied simple HV grid with SG.

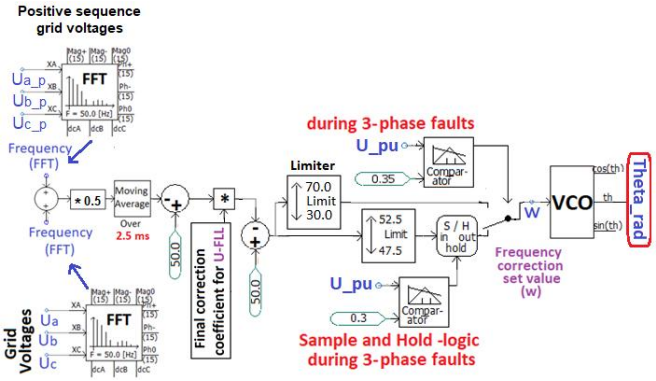

Figure 2. Studied further modified U-FLL component of 20 MW BESS, see also Fig. 1 and Table I.

It should be also noted (Fig. 1 and Tables I and II) that while BESS's nominal total capacity is 20 MW (5*4 MW), GFM PV unit [15] with 40 MW nominal capacity has 20 MW output just before the disturbance i.e. load changes at t=10.0 s in the simulations. The total simulation time in the study cases (Tables I and II) is t=20.0 s and load increase (100 MW) at t=10.0 s happens at the end of 50 km HV feeder (Fig. 1). Load was 505.5 MW before the 100 MW load increase.

In Fig. 4, the PV GFM PSCAD module from [15] and the used input parameters of it are presented. Fig. 5 shows the base control parameters of the PV GFM (Fig. 4) that have been used in the simulations of this paper (Table II) with the four GFM control methods (i.e. SRF-PLL, Droop, VSM and dVOC). It can be also noted that the PV GFM model from [15] consists of scaled 250 kW detailed PV unit model that is presented in Fig. 4.

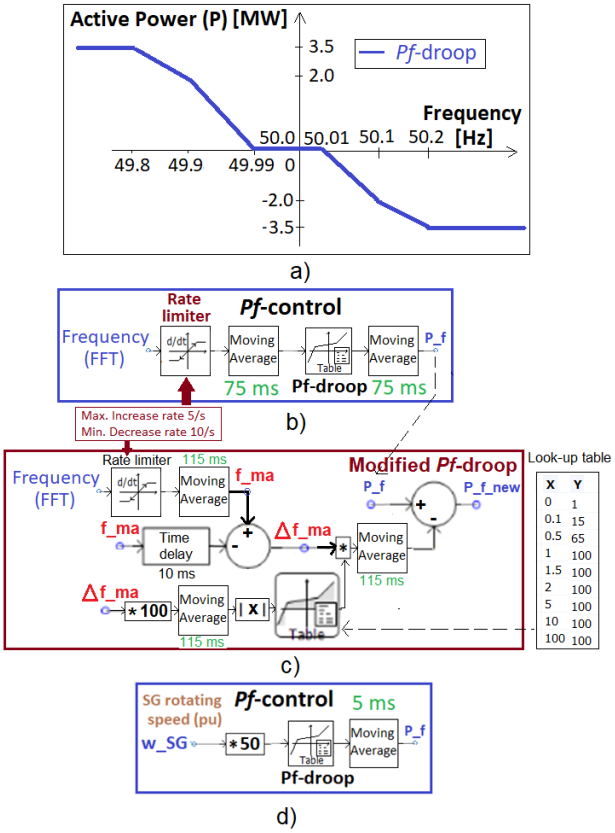

Figure 3. a) 20 MW (5*4 MW) BESS's *Pf*-droop settings for one 4 MW BESS unit, b) input frequency filtering including moving averaging (75 + 75 ms) and rate limiter of the BESS's *Pf*-droop control when the input frequency is coming from the FFT -block of PSCAD like in [10], c) BESS's further modified *Pf*-droop utilization from Fig. 3b) and [10] and d) input frequency filtering (5 ms moving average) of the BESS *Pf*-droop control when the input comes from SG speed like in [10] (see Fig. 1 and Table I).

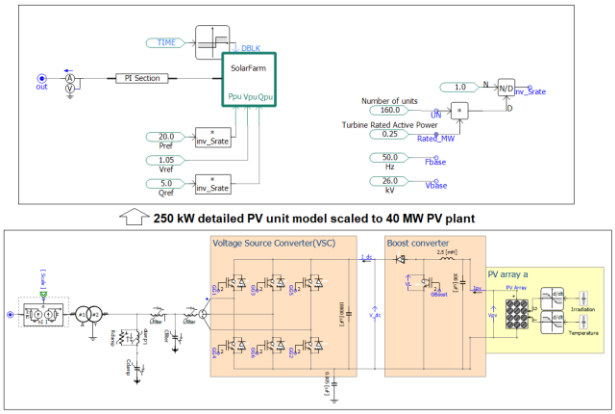

Figure 4. 40 MW GFM PV plant from [15] consisting of scaled 250 kW detailed PV unit model (see Fig. 1, 5 and Table II).

The key PSCAD simulation cases of this paper are presented in Tables I and II. In Table I, the study cases to compare effects of different 20 MW BESS's U-FLL and *Pf*-control modifications on frequency stability support after the load increase are shown (see Figs. 1-3). Respectively, Table II presents the study cases to compare the effect of four different GFM control methods of 40 MW PV on frequency stability support after the load increase (see Figs. 1, 4 and 5).

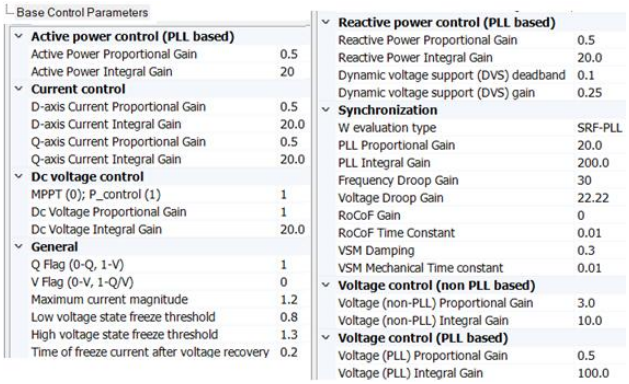

Figure 5. Base control parameters of the PV GFM with the four different GFM control methods SRF-PLL, Droop, VSM and dVOC (see Fig. 1 and 4 & Table II).

TABLE I
STUDY CASES TO COMPARE THE EFFECT OF DIFFERENT 20 MW BESS'S U-FLL AND *PF*-CONTROL MODIFICATIONS ON FREQUENCY SUPPORT (SEE FIGS. 1-3)

Case	20 MW BESS with U-FLL	
	U-FLL properties	**Active power *P* control**
BASE CASE_A	U-FLL corr. coefficient = 1 (GFL)	No *Pf*-control
BASE CASE_B	U-FLL corr. coefficient = 1 (GFL), input freq. of U-FLL from SG speed	No *Pf*-control
CASE_1_A**)	U-FLL corr. coefficient = 1 (GFL)	*Pf*-control
CASE_1_B*)	U-FLL corr. coefficient = 1 (GFL), input freq. of U-FLL from SG speed	*Pf*-control, input freq. of *Pf*-control from SG speed
CASE_2_A***)	U-FLL adaptive corr. coefficient (GFM)	Modified *Pf*-control

*) *Input freq. of the Pf-control (Fig. 1) from SG speed (mov. aver. 5 ms, see Fig. 3d),* **) *Input freq. of the Pf-control (Fig. 1) from FFT -block of PSCAD (mov. aver. 75+75 ms, see Fig. 3b),* ***) *Modified Pf-control, see Fig. 3c*

TABLE II
STUDY CASES TO COMPARE THE EFFECT OF FOUR DIFFERENT 40 MW PV'S GFM CONTROL METHODS ON FREQUENCY SUPPORT (SEE FIGS. 1, 4 AND 5)

Case	GFM control method
CASE_3 (SRF-PLL)	SRF-PLL
CASE_3 (Droop)	Droop
CASE_3 (VSM)	VSM
CASE_3 (dVOC)	dVOC

III. RESULTS OF THE SIMULATIONS

In this Section III, key results of the PSCAD simulations from the study cases of Tables I and II are shown. First, in Figs. 6-9 results from the study cases of Table I are presented. After that, Figs. 10-13 show the simulation results from Table II study cases as well as from two chosen Table I cases. It should be noted that in Table I study cases only CASE_2_A has GFM capability due to used adaptive U-FLL correction coefficient (Fig. 2) which means that in case of 100 % IBR-based power systems steady-state frequency deviation will not exist (see [7]) unlike in the other Table I study cases with U-FLL correction coefficient 1. Therefore, these other cases are marked in Table I with GFL instead of GFM. However, when U-FLL corr. coefficient = 1 the 100 % IBR-based system with U-FLL synchronized IBRs can be still maintained stable but there exists steady-state frequency deviation which exists also with typical GFM control methods like Droop -control.

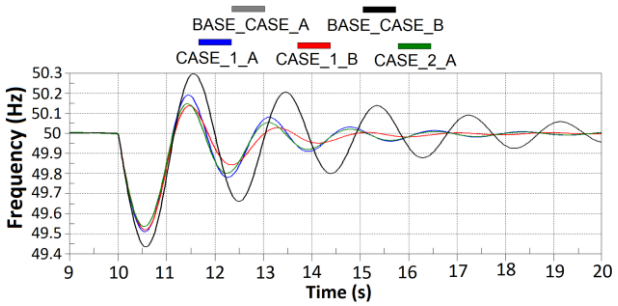

Figure 6. Determined frequency from SG's rotor speed after 100 MW load increase (t=10.0 s) in Table I study cases.

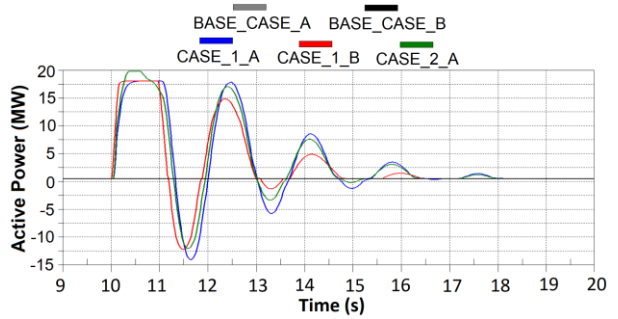

Figure 7. Active power P of 20 MW BESS after 100 MW load increase (t=10.0 s) in Table I study cases.

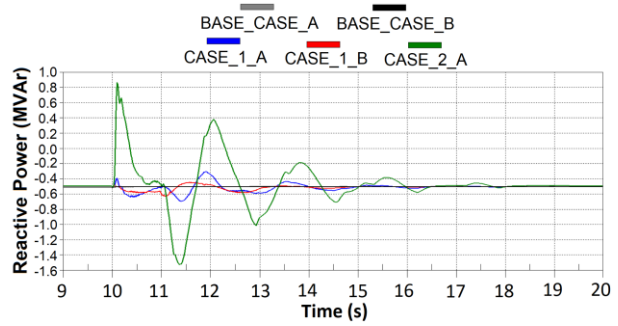

Figure 8. Reactive power Q of 20 MW BESS after 100 MW load increase (t=10.0 s) in Table I study cases.

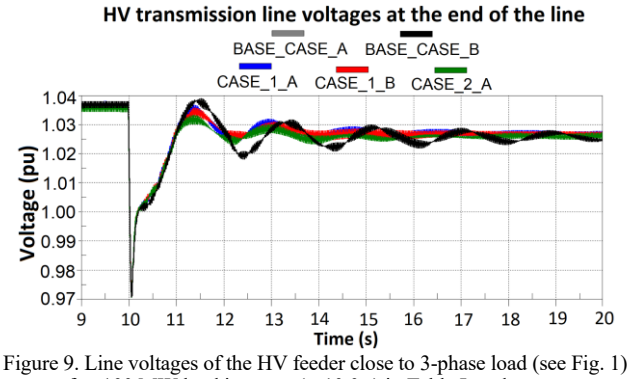

Figure 9. Line voltages of the HV feeder close to 3-phase load (see Fig. 1) after 100 MW load increase (t=10.0 s) in Table I study cases.

From Fig. 6 it one can see that frequency nadir in BASE CASE_A and BASE CASE_B is 49.435 Hz i.e. 0.565 Hz below nominal 50 Hz frequency. Respectively, frequency deviation from 50 Hz during frequency nadir is in CASE_1_A 0.488 Hz (13.7 % reduction from the BASE CASEs), in CASE_1_B 0.48 Hz (15.0 % reduction from BASE CASEs) and in CASE_2_A 0.463 Hz (18.1 % reduction from BASE CASEs). Fig. 6 shows that the most stable Table I cases are CASE_1_B and CASE_2_A in terms of frequency stability after the 100 MW load increase (t=10.0 s). One can also see from Fig. 6 that frequency stability is better when having input frequency coming directly from the rotating speed of SG (Fig. 1) for the 20 MW U-FLL-based BESS's U-FLL synchronization and *Pf*-droop control in CASE_1_B (Table I). In addition, Fig. 6 shows that proposed modified *Pf*-droop control (Fig. 3c) used in CASE_2_A can improve the frequency stabilization during the first swings when compared to CASE_1_A. Fig. 7 shows P and Fig. 8 Q of 20 MW BESS after the 100 MW load increase (t=10.0) s in Table I simulation cases. Fig. 7 illustrates that in CASE_1_B the P response after the load increase is the fastest. In addition, one can see from Fig. 8 that in CASE_2_A with U-FLL adaptive correction coefficient (Fig. 2, Table I) the reactive power Q of 20 MW BESS oscillates the most. Therefore, it could be concluded that the U-FLL-based BESS's Q oscillations are dependent, not only on the power system frequency behaviour after the load increase, but also on the use of adaptive U-FLL correction coefficient.

It can be seen from Fig. 10 that when comparing Table II cases with different GFM control methods and their base control parameters (Fig. 5) on 40 MW PV (Fig. 4), CASE_3 (dVOC) is the most stable and CASE_3 (SRF-PLL) the least stable. However, CASE_3 (Droop) and CASE_3 (VSM) provide almost similar frequency behavior (Fig. 10) when compared to CASE_3 (dVOC) due to their nearly same active P (Fig. 11) and reactive power Q (Fig. 12) response after the 100 MW load increase (t=10.0 s). Still, both P (Fig. 11) and especially Q (Fig. 12) responses in CASE_3 (dVOC) are higher and better than in CASE_3 (Droop) and CASE_3 (VSM). From Fig. 11 and 12 one can see also that in CASE_3 (SRF-PLL) the P and especially Q response is very different when compared to the other cases (i.e. CASE_3 (Droop), CASE_3 (VSM) and CASE_3 (dVOC). In the other cases with Droop, VSM or dVOC control both P (Fig. 11) and Q (Fig. 12) output of GFM PV oscillate according to the frequency oscillations (Fig. 10). However, the direction of Q in cases with Droop, VSM or dVOC control seems to be (Fig. 12) so that during, for example, the first under-frequency swing (Fig. 10) the PV draws a high amount of Q from the power system. From the voltage stability support (Fig. 13) viewpoint, after the 100 MW load increase (t=10.0 s), this high drawn Q may be questionable. In Fig. 12, also the amount of reactive power Q drawn or fed by PV GMFs in CASE_3 (Droop), CASE_3 (VSM) and CASE_3 (dVOC) may seem quite high during the first oscillations when compared to the active power P of the PV GFMs in Fig. 11. However, this is because PV does not provide nominal or maximum 40 MW active power P before the disturbance.

Regarding simulation results of Figs. 10-13, one could note that the used base control parameters of the PV GFM (Fig. 5) in the Table II study cases also affect the results and base control parameters optimization to achieve the best possible frequency support by the compared GFM methods has not been done in this paper.

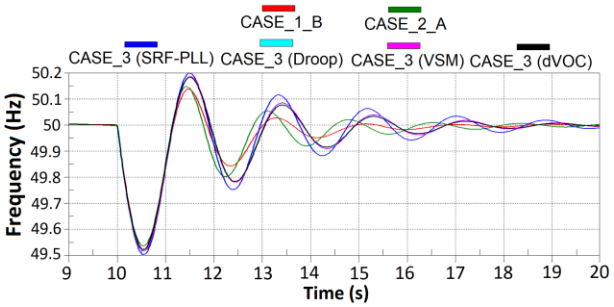

Figure 10. Determined frequency from SG's rotor speed after 100 MW load increase (t=10.0 s) in two Table I and all Table II study cases.

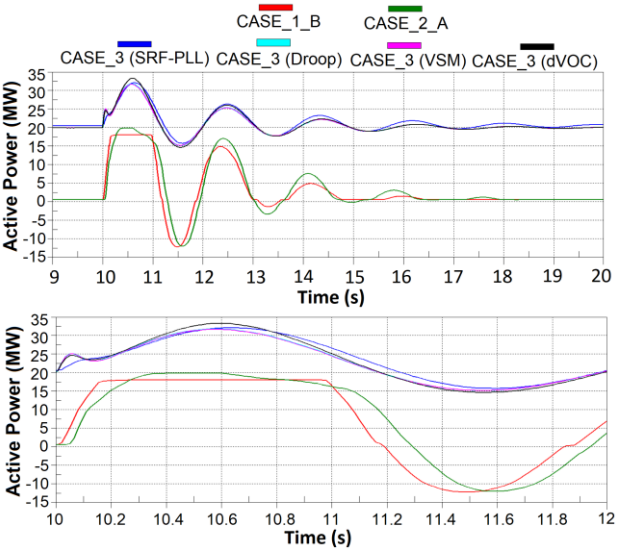

Figure 11. Active power P of 40 MW GFM PV and 20 MW BESS after 100 MW load increase (t=10.0 s) in two Table I and all Table II study cases.

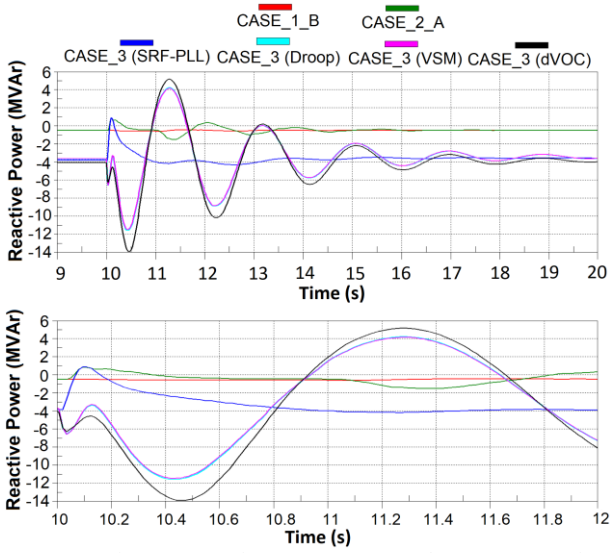

Figure 12. Reactive power Q of 40 MW GFM PV and 20 MW BESS after 100 MW load increase (t=10.0 s) in two Table I and all Table II study cases.

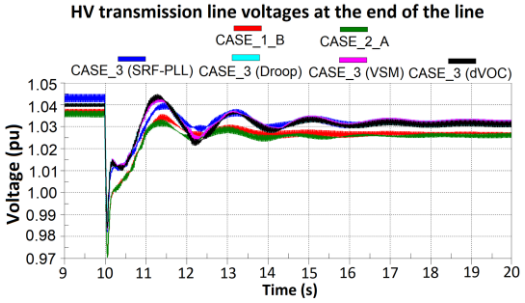

Figure 13. Line voltages of the HV feeder close to 3-phase load (see Fig. 1) after 100 MW load increase (t=10.0 s) in two Table I and all Table II cases.

When comparing P response of 20 MW BESS in Table I cases CASE_1_B and CASE_2_A with the P response of 40 MW PV in Table II cases, Fig. 11 shows that CASE_1_B can provide the most stable P response during the first swing after the 100 MW load increase (t=10.0 s). Therefore, the frequency stability support (Fig. 10) is also best in this case CASE_1_B. However, the amount of active power P that can be fed after the load increase to support the frequency is higher with the 20 MW BESS than with the GFM controlled 40 MW PV (Fig. 11) and this naturally has an effect on the provided frequency stability support.

IV. Conclusions

In the future, increasing amount of rapid support for the frequency control and stability in the power systems with low-inertia is required from IBR-based DERs both during normal operation and disturbances. Therefore, modification or rethinking of the existing markets and grid codes for improved involment of very fast and stable frequency as well as synchronization support from different type and size of DER units can be needed. It should be clearly defined what sort of grid-supporting or -forming functionality is needed also from the IBRs connected in LV and MV distribution grids so that these requirements would be compatible with the future DSO operation, control and protection schemes as well as that they are coordinated and prioritized in collaboration with the TSO to ensure the resiliency of the future power systems.

In this paper, U-FLL-based synchronization and *Pf*-droop control of IBRs has been further studied to achieve better frequency stability support. In addition, frequency stability comparison between four different GFM control methods (SRF-PLL, Droop, VSM and dVOC) were done. PSCAD simulation model of small power system with SG and BESS or GFM PV to study their effect on the power system frequency stability after a load increase was used in the studies. Following conclusions and notifications were done from the cases with the U-FLL-based BESS:

- Frequency stability was improved when the input frequency for U-FLL component and *Pf*-droop control was coming from the SG rotating speed.
- Further modified *Pf*-droop control can improve the frequency stabilization during the first swings. For example, frequency deviation from 50 Hz during frequency nadir was reduced 5 % with the further modified *Pf*-control in CASE_2_A from the CASE_1_A.
- U-FLL-based BESS's Q oscillations were dependent also on the use of adaptive U-FLL correction coefficient.

Similarly, following conclusions and notifications were made from the study cases with GFM PV when comparing different GFM control methods:

- dVOC was the most stable and SRF-PLL the least stable. However, Droop and VSM provided almost similar frequency support and behavior. In the future studies, also GFM base control parameters optimization could be done to see if it would affect the behavior and ranking of different GFM methods.

In general, the studied power system was quite simple and therefore in future studies larger and more complex power systems with different shares of various IBRs should be also studied. From the voltage stability support viewpoint, the high reactive power Q taken from the power system after the load increase, when using Droop, VSM or dVOC control on the PV inverter, may be questionable and should be further studied together with optimized GFM control parameters simulations also after major disturbances like 3-phase faults.

Acknowledgments

This study was done as a part of Business Finland funded "Smart Grid 2.0" -project (Grant No. 1386/31/2022).

References

[1] J. Marchand, J. Buire, V. Debusschere, N. E. Jarrai, J. Pompée, and N. Hadjsaid, "Large-Signal Stability of Inverter-Based LV Microgrids: Share of Grid-Forming Units," in Proc. *ISGT Europe 2023*, Grenoble, France, 2023.

[2] A. Shrestha, and F. Gonzalez-Longatt, "Frequency Stability Issues and Research Opportunities in Converter Dominated Power System," *Energies*, vol. 14, 2021.

[3] R. Musca, A. Vasile, and G. Zizzo, "Grid-forming converters. A critical review of pilot projects and demonstrators," *Renewable and Sustainable Energy Reviews*, vol. 165, 2022.

[4] N. Mohammed, H. H. Alhelou, and B. Bahrani, "Grid-Forming Power Inverters - Control and Applications," *CRC Press*, 2023.

[5] R. Musca, F. Gonzalez-Longatt, and C. A. Gallego Sánchez, "Power System Oscillations with Different Prevalence of Grid-Following and Grid-Forming Converters," *Energies*, vol. 15, 2022.

[6] D. B. Rathnayake et al., "Grid Forming Inverter Modeling, Control, and Applications," *IEEE Access*, vol. 9, 2021.

[7] H. Laaksonen, "Universal Grid-forming Method for Future Power Systems," *IEEE Access*, vol. 10, 2022.

[8] H. Laaksonen, "Improvement of Power System Frequency Stability With Universal Grid-Forming Battery Energy Storages," *IEEE Access*, vol. 11, 2023.

[9] H. Laaksonen, "Solutions to Improve Transient Stability of Universal Grid-forming Inverter-based Resources," *Int. Review of Electrical Engineering (IREE)*, vol. 18, no. 3, pp. 164–179, 2023.

[10] H. Laaksonen, "Stability of Future Low-Inertia Power Systems with Different Grid-Forming Control Schemes," in Proc. *CIRED 2024 Workshop*, Vienna, Austria, 2024.

[11] H. Laaksonen, and N. Hatziargyriou, "Reconnection of MV Microgrid with Universal Grid-forming Inverter-based Resources," in Proc. *MedPower 2024*, Athens, Greece, 2024.

[12] H. Laaksonen, H. Khajeh, and N. Hatziargyriou, "Advanced Distributed Energy Resources and On-Load Tap-Changer Control Principles for Enhanced Flexibility Services Provision," *IEEE Access*, vol. 12, 2024.

[13] H. Laaksonen, H. Khajeh, and N. Hatziargyriou, "Novel DER and OLTC Management Scheme for Coordinated TSO-DSO Flexibility Services Provision," in *ISGT Europe 2023*, Grenoble, France, 2023.

[14] H. Laaksonen, and N. Hatziargyriou, "Frequency-dependent Control of DERs and OLTCs in the Future Distribution Networks," in Proc. *CIRED 2025 Conference*, Geneva, Switzerland, 2025.

[15] PSCAD, Manitoba Hydro International, "EPRI Grid Forming Inverter Models," 2022.